

# Flatness of Minima in Random Inflationary Landscapes

Yang-Hui He<sup>a,b,c,\*</sup>, Vishnu Jejjala<sup>d,†</sup>, Luca Pontiggia<sup>d,‡</sup>, Yan Xiao<sup>a,§</sup>, Da Zhou<sup>a,e,¶</sup>

<sup>a</sup> *Department of Mathematics, City, University of London,  
Northampton Square, London EC1V 0HB, UK*

<sup>b</sup> *Merton College, University of Oxford, OX1 4JD, UK*

<sup>c</sup> *School of Physics, NanKai University, Tianjin, 300071, P.R. China,*

<sup>d</sup> *Mandelstam Institute for Theoretical Physics, NITheP, CoE-MaSS, and School of Physics,  
University of the Witwatersrand, Johannesburg, WITS 2050, South Africa*

<sup>e</sup> *The Interdisciplinary Center for Theoretical Study,  
University of Science and Technology of China, Hefei, Anhui, 230026, China*

## Abstract

We study the likelihood which relative minima of random polynomial potentials support the slow-roll conditions for inflation. Consistent with renormalizability and boundedness, the coefficients that appear in the potential are chosen to be order one with respect to the energy scale at which inflation transpires. Investigation of the single field case illustrates a window in which the potentials satisfy the slow-roll conditions. When there are two scalar fields, we find that the probability depends on the choice of distribution for the coefficients. A uniform distribution yields a 0.05% probability of finding a suitable minimum in the random potential whereas a maximum entropy distribution yields a 0.1% probability.

---

\*hey@maths.ox.ac.uk

†vishnu.jejjala@gmail.com

‡lucapontiggia@gmail.com

§Yan.Xiao@city.ac.uk

¶zhouda@mail.ustc.edu.cn

# Contents

<b>1</b>	<b>Introduction</b>	<b>2</b>
<b>2</b>	<b>Random potentials for inflation</b>	<b>4</b>
<b>3</b>	<b>Single field models</b>	<b>6</b>
3.1	Behavior of slow-roll parameters . . . . .	8
3.1.1	$\beta \geq 0.7789$ . . . . .	10
3.1.2	$0.6021 \leq \beta < 0.7789$ . . . . .	11
3.1.3	$9/32 \leq \beta < 0.6021$ . . . . .	11
3.1.4	$1/4 < \beta < 9/32$ . . . . .	12
3.1.5	$0 < \beta \leq 1/4$ . . . . .	13
3.2	The window . . . . .	13
<b>4</b>	<b>Multi-field models</b>	<b>14</b>
4.1	Slow-roll conditions for multi-field inflation . . . . .	15
4.2	Numerical tests . . . . .	16
4.2.1	Setup for numerics . . . . .	16
4.2.2	Numerical results . . . . .	18
<b>5</b>	<b>Discussion and outlook</b>	<b>21</b>

# 1 Introduction

In order to solve the well known horizon and flatness problems, cosmological inflation [1–4] posits that the Universe underwent a period of exponential expansion early in its history (at around  $t_{\text{GUT}}$ ). To date, there is no uniquely compelling realization of how inflation transpired. The literature abounds with numerous and varied proposed mechanisms [5, 6]. Paradigmatic models involve scalar fields which dynamically roll until arriving at the (relative) minimum of some potential.

While a model of physics that purports to approximate our world must correctly trace out the cosmological history of the Universe, these are not the only considerations in selecting a theory. The Standard Model of particle physics establishes that at low energies the particles in Nature organize themselves into three generations of chiral fields that transform in representations of the  $SU(3) \times SU(2)_L \times U(1)_Y$  gauge group. Top down realizations of low energy gauge theories from a fundamental theory such as string theory typically augment the symmetries of the S-matrix with supersymmetry. The simplest scenario for preserving  $\mathcal{N} = 1$  supersymmetry in four dimensions involves the compactification of the heterotic string in ten dimensions on a Calabi–Yau threefold [7]. This effort has led to a number of constructions that reproduce the matter spectrum and Yukawa interactions observed in the Standard Model [8–12]. Again, we have an abundance of models that are *a priori* indistinguishable on the basis of experiments.

As we do not have a *sui generis* path to the real world, we propose to study a large class of models at once and incorporate inputs of both cosmology and particle physics. The most important characterization of a Calabi–Yau threefold is a pair of topological invariants  $h^{1,1}$  and  $h^{2,1}$ . There are  $h^{1,1}$  Kähler and  $h^{2,1}$  complex structure parameters that describe the size and the shape of the geometry. In the most naïve setup, these deformation parameters supply candidates for the scalar fields in inflation. The largest available catalog of Calabi–Yau threefolds is derived from the Kreuzer–Skarke database of reflexive polytopes [13, 14]. Using the methods of Batyrev and Borisov [15, 16], each consistent triangulation of a reflexive polytope yields a toric Calabi–Yau manifold. In [17, 18], topological and geometric data are tabulated for the Calabi–Yau threefolds thus obtained for low values of  $h^{1,1}$ . Heterotic Standard Model constructions in string theory typically employ Calabi–Yau geometries with small values of the Hodge numbers. For example, [8] uses a manifold with  $(h^{1,1}, h^{2,1}) = (3, 3)$ . Where there are explicit candidates for particle physics from string theory, we expect only a small number of moduli to appear in the low energy effective action. Motivated by this fact, these are the models that we investigate in

this article.

We aim to provide statistics for how many (possibly metastable) vacua support slow-roll constraints on inflation. Working in effective field theory, we examine random polynomial potentials for inflation with a small number of scalar fields. The potentials we study are sums of monomials in the scalar fields. We truncate the expansion to focus on the interactions that are relevant or marginal from the perspective of a four dimensional low energy effective action. As higher order monomials in the fields are irrelevant operators, we expect these to be mass suppressed and neglect them for the purposes of our investigations. Corresponding to the time scale for inflation, the energy scale in the problem is  $M_{\text{GUT}}$ . Invoking naturalness [19], we choose coefficients in the potential to be order one with respect to this scale. In discussing single field models with order one coefficients, our work is analytic. In multi-field models, we construct random potentials whose coefficients are selected from distributions.

At the outset, we should note that the cases we analyze where there are few moduli may well represent an atypical class of string compactifications. While there are 473 800 776 reflexive polyhedra in four dimensions, there are only 30 108 pairs of Hodge numbers that appear in the threefold dataset. The number of reflexive polytopes in the Kreuzer–Skarke list peaks at the Hodge numbers  $(h^{1,1}, h^{2,1}) = (27, 27)$ . There are 910 113 such polytopes. Indeed, there are significant and surprising patterns in the distribution of Calabi–Yau geometries close to this maximum [20]. Reflexive polytopes with low Hodge numbers are sparse in the Kreuzer–Skarke database. Flux compactifications on Calabi–Yau threefolds yield, in principle, an enormously large number of potential vacua for string theory [21, 22]. There are, however, to date no explicit constructions of the Standard Model on a geometry with Hodge numbers that correspond to those of a typical Calabi–Yau manifold. As there are good reasons to be skeptical about anthropic resolutions to the cosmological constant problem and there are potential issues regarding the stability of the flux vacua [23–25], we adopt an agnostic attitude. We simply note that if a construction is stable in this context, a generic compactification on a typical Calabi–Yau manifold will most likely involve a large number of moduli fields. As we review below, the large- $N$  limit of inflaton fields is studied in complementary work.

The organization of the paper is as follows. In Section 2, we discuss the setup for random inflation. In Section 3, we investigate the case of single field inflation with  $O(1)$  coefficients. This analysis is a completely analytic study of polynomial equations. In Section 4, we examine the case of two scalar fields with couplings up to quartic order. Again, the coefficients are  $O(1)$ . We choose coefficients using a uniform distribution and a Gaussian distributions for coefficients

of indefinite sign and a gamma distribution for coefficients that are positive. In Section 5, we remark on future investigations in the context of semi-realistic string models.

## 2 Random potentials for inflation

The action we consider assumes the form

$$I = - \int d^4x \sqrt{-g} \left( \frac{R}{16\pi G} + \frac{1}{2} g^{\mu\nu} \partial_\mu \phi \cdot \partial_\nu \phi - V(\phi) \right), \quad (1)$$

where the Einstein–Hilbert term is supplemented by a matter sector that consists of  $k$  scalar fields,

$$\phi = (\phi^1, \phi^2, \dots, \phi^k). \quad (2)$$

For simplicity, we assume that the metric in field space is the identity matrix, *i.e.*,

$$\partial_\mu \phi \cdot \partial_\nu \phi = \delta_{ij} \partial_\mu \phi^i \partial_\nu \phi^j. \quad (3)$$

The scalar potential  $V(\phi)$  determines the model and can be expanded as a polynomial in the fields  $\phi^i$ .

This setup lets us examine cosmological inflation. Deducing the form of the potential is a long standing problem; many scenarios present attractive phenomenological features, and to date observation has provided only limited guidance in selecting  $V(\phi)$ . In models with a single inflation field, famously the WMAP [26] and Planck [27] observations disfavor the simplest quadratic potential. Other scenarios are variously consistent with the data. See, for example, [28] for a recent review.

One of the simplest multi-field models, hybrid inflation [29], involves coupling two fields according to the potential

$$V(\phi, \psi) = \frac{1}{4\lambda} (\lambda\psi^2 - M^2)^2 + \frac{1}{2} m^2 \phi^2 + \frac{\lambda'}{2} \phi^2 \psi^2. \quad (4)$$

Here,  $\lambda$  and  $\lambda'$  are couplings and  $M$  and  $m$  are the masses of  $\psi$  and  $\phi$ , respectively. We require that  $V(\phi) = \frac{1}{2} m^2 \phi^2 \ll \frac{M^4}{4\lambda}$ . This guarantees that the inflationary energy density of the false vacuum associated to the symmetry breaking potential  $V(\psi) = \frac{\lambda}{4} (\psi^2 - M^2)^2$  dominates. The effective mass for the  $\psi$  field is  $M_{\text{eff}}^2 = -M^2 + \lambda' \phi^2$ , which vanishes at  $\phi_*^2 = M^2/\lambda'$ . Starting from  $\phi^2 \gg M^2$ , the minimum is at  $\psi = 0$ . This is morally a single field model with an effective potential of the form

$$V_{\text{eff}} = \frac{\lambda}{4} M^4 + \frac{1}{2} m^2 \phi^2. \quad (5)$$

The field rolls until it reaches  $\phi_*$ . The  $\psi = 0$  locus is then unstable, and the field rolls again into the true minima at  $\phi = 0$ ,  $\psi = \pm M$ . Interest in the model stems from its versatility and success in predicting certain features of inflation, such as the power law behavior of the perturbation spectrum. By tweaking the model in various ways, one can deal with inflation with or without first order phase transitions. While this is a prototype multi-field model, there is a built-in hierarchy to the coefficients. (See also [30].)

By constraining the inflationary scenario at a level matching the accuracy of current experimental data, [6] presents an encyclopedia of 74 satisfactory models. In our work, we adopt a slightly different approach and address the question of how generic or specific the models should be in order to satisfy experimental constraints. For this purpose, we consider randomly generated multi-field models (with the inflationary potential being given by polynomials with random coefficients) and verify whether the models can satisfy a certain set of conditions. In particular, we demand that the scalar potential has a parameter window such that slow-roll conditions are satisfied.

Suppose there are some minima that satisfy the slow-roll conditions. What are the global features of the potentials that accommodate this? Turning the question around, given a large set of potentials (which may have some distribution in the function space), how likely is it that the potential has regions that satisfy slow-roll conditions? How often can slow-roll inflation be accommodated with  $O(1)$  coefficients? These are the issues we aim to address below.

In an analysis of multi-field inflation, the need to establish the behavior of random potentials is almost compulsory. Generic compactifications, can have hundreds of scalar fields [31–34]. Since these theories describe physics at energy scales close to the inflationary scale, there is considerable interest in analyzing their dynamics. Considering random potentials with large- $N$  fields has a considerable history [35–47]. As multi-field models have an almost infinite number of ways to inflate, the task of understanding how the potential energy driving inflation is distributed among all these fields becomes an incredibly difficult one. This problem is often referred to as the measure problem, and it deals with attempting to handle the possible initial conditions [48–51]. Multidimensional landscapes may also be afflicted by instabilities [52–54]. In general, the approach that random multi-field inflation adopts, is to study the dynamics of inflation by creating an ensemble of random potentials. Then, through a statistical analysis, one can comment on the inflationary landscape produced by the respective models. Related studies have recently appeared in the context of Gaussian models [55, 56] and non-minimal kinetic terms [57].<sup>1</sup>

---

<sup>1</sup> As we were completing this work, a similarly themed investigation appeared in [58]. This work examines

The study of random potentials is of course not limited to inflation. It is useful to borrow techniques for the generation of random potentials from other fields in physics, in particular string theory and quantum field theory [59, 60], and adapt these ideas to the cosmological context.

In Section 3, we analyze the single field case analytically. In Section 4, we investigate the statistics of random inflation by examining a large set of sample potentials for two field inflation. In each potential, the coefficients are random numbers that fall within a particular range. For each sample potential, we examine whether it has slow-roll regions. We calculate the fraction of potentials that do have slow-roll regions and examine what features they have in common. For succinctness, in the following we will use the term “*slow-roll potentials*” to refer to those potentials that satisfy the slow-roll conditions in some region of the field space. We assume the potential term  $V(\phi)$  is a polynomial in  $\phi^i$  up to degree four and is bounded below. In this paper, we only consider single field and two field inflation models. In the former case, we shall denote  $\phi = \tilde{\varphi}$ , and in the latter,  $\phi = (\tilde{\varphi}, \tilde{\psi})$ . Both cases are developed in the following sections.

### 3 Single field models

The polynomial potential up to degree four for single field inflationary models has the form

$$V_{a,b}(\tilde{\varphi}) = \frac{\tilde{\varphi}^2}{2}(M^2 - aM\tilde{\varphi} + b\tilde{\varphi}^2) , \quad (6)$$

where  $M \lesssim 10^{16}$  GeV is the mass of the inflaton  $\tilde{\varphi}$ , and  $a$  and  $b$  are two dimensionless random numbers. Note that in order for the potential to be bounded from below, the quartic term must be positive, which means we presume  $b$  is positive. Another feature about this potential is the symmetry

$$V_{-a,b}(\tilde{\varphi}) = V_{a,b}(-\tilde{\varphi}) , \quad (7)$$

which indicates if  $V_{a,b}$  is a slow-roll potential,  $V_{-a,b}$  must also be slow-roll. So again we only need to assume that  $a$  is positive.

Now, to factor out the parameter  $M$ , we perform a rescaling,  $\tilde{\varphi} = M\varphi$ , which also makes  $\varphi$  dimensionless. Then the potential can be recast as

$$V(\varphi) = \frac{M^4}{2}\varphi^2(1 - a\varphi + b\varphi^2) , \quad (8)$$

---

inflationary landscapes corresponding to one dimensional potentials.

where we have omitted the two subscripts  $a$  and  $b$  on  $V$ . Consequently, the two slow-roll parameters are

$$\begin{aligned}\epsilon &= \frac{M_{\text{Pl}}^2}{2} \left( \frac{V'(\tilde{\varphi})}{V(\tilde{\varphi})} \right)^2 = \frac{1}{2\mu} \left( \frac{V'(\varphi)}{V(\varphi)} \right)^2, \\ \eta &= M_{\text{Pl}}^2 \frac{V''(\tilde{\varphi})}{V(\tilde{\varphi})} = \frac{1}{\mu} \frac{V''(\varphi)}{V(\varphi)},\end{aligned}\tag{9}$$

where  $M_{\text{Pl}}$  is the Planck mass and  $\mu = M^2/M_{\text{Pl}}^2$  is the square of the ratio between the mass of the inflaton and the Planck mass. The Planck 2015 [28] data tells us that the scalar spectral index is measured to be  $n_s = 0.9655 \pm 0.0062$  and the slow-roll parameters are deduced to satisfy

$$\epsilon < 0.012, \quad \eta = -0.0080^{+0.0088}_{-0.0146}.\tag{10}$$

Noting that  $n_s - 1 = 2\eta - 6\epsilon$ , in our analysis we demand that the slow-roll parameters are  $O(10^{-2})$ :

$$\epsilon < 0.01, \quad |\eta| < 0.01.\tag{11}$$

Given the definition of  $\mu$ , the two slow-roll parameters are actually independent of the specific value of inflaton mass  $M$  because the  $M^4$  term in (8) appears in both the numerator and denominator of (9) and therefore cancels.

If we define a new variable  $y = a\varphi$ , the whole analysis will only depend on the ratio of  $b$  to  $a^2$ , which shall be dubbed  $\beta$ , instead of the explicit values of  $a$  and  $b$ . So we can define an auxiliary potential,

$$v(y) = \frac{2a^2}{M^4} V(\varphi) = y^2(1 - y + \beta y^2), \quad \beta = \frac{b}{a^2} > 0,\tag{12}$$

and two new slow-roll parameters which only depend on one parameter  $\beta$ ,

$$\bar{\epsilon} = \frac{1}{2} \left( \frac{v'}{v} \right)^2 = \frac{\nu}{0.01} \epsilon, \quad \bar{\eta} = \frac{v''}{v} = \frac{\nu}{0.01} \eta,\tag{13}$$

where

$$v' \equiv \frac{dv}{dy}, \quad v'' \equiv \frac{d^2v}{dy^2}, \quad \nu \equiv \frac{0.01\mu}{a^2} = \frac{0.01}{a^2} \frac{M^2}{M_{\text{Pl}}^2}.\tag{14}$$

The slow-roll conditions become

$$\bar{\epsilon} < \nu, \quad |\bar{\eta}| < \nu.\tag{15}$$



Of course, we have assumed  $a \neq 0$  in (12) and (15), and the special  $a = 0$  case can be approximated by setting  $a$  to be an extremely small nonzero number, then  $a \rightarrow 0$  corresponds to the  $\beta \rightarrow \infty$  case, which is a special situation that will be discussed in Section 3.1.1.

From (12) one can see that as  $y \rightarrow \pm\infty$ ,  $v \sim y^4$  while  $v' \sim y^3$  and  $v'' \sim y^2$ , so (11) is always satisfied. That means, there exists a  $y_0 > 0$  and a  $y'_0 < 0$  such that (11) holds true for all  $y > y_0$  or all  $y < y'_0$ . In other words, in any cases there are always at least two trivial slow-roll regions,  $(-\infty, y'_0)$  and  $(y_0, \infty)$ . However, in a realistic inflationary scenario these two regions are not ideal slow-roll regions that propel the Universe to inflate because (11) is satisfied simply due to the largeness of the potential  $v$  whereas more realistic models would prefer a flat  $v$  (*i.e.*, small  $v'$  and  $v''$ ) during inflation. Hence in the following analysis, we shall ignore these two obvious and unrealistic slow-roll regions and concentrate on regions in which  $v$  is flat enough. In the previous argument, there is not a trivial way to define what “flat enough” means. Therefore, in this paper, we adopt a naïve procedure to pick “flat” slow-roll regions, which is simply excluding these two infinite domains. That is, any region of finite length shall be deemed flat.

From (13) we have

$$\frac{d\bar{\epsilon}}{dy} = \frac{v'}{v^3}(v''v - v'^2) = -\frac{y^2}{v^3}v'[2 - 4y + (3 + 2\beta)y^2 - 6by^3 + 4\beta^2y^4]. \quad (16)$$

For  $y < 0$ , we have  $v > 0$ ,  $v' < 0$ , and the expression within the brackets is positive, so  $\frac{d\bar{\epsilon}}{dy} > 0$ . This means, if we find a  $y'_0 < 0$  such that  $\bar{\epsilon}(y'_0) = 0.01$ , then  $(-\infty, y'_0)$  is a trivial slow-roll region and  $(y'_0, 0)$  does not contain a non-trivial slow-roll region. Hereafter, we are only interested in the region with  $y > 0$ .

In deducing the regions that satisfy the slow-roll conditions in single field inflation, we do not need to perform a Monte Carlo analysis or scan over potentials with random coefficients. It suffices to analytically examine a system of polynomial equations. We do this in the following subsection. Different intervals for  $\beta$  exhibit characteristic behavior.

### 3.1 Behavior of slow-roll parameters

Graphically, we can draw the slow-roll parameters, which are functions of  $y$  given a specific value of  $\beta$ , on the plane and use the horizontal lines  $\bar{\epsilon} = \nu$  and  $\bar{\eta} = \pm\nu$  to intercept curves of the slow-roll parameters  $\bar{\epsilon}$  and  $\bar{\eta}$  respectively, then from the interception one can easily read off whether there are slow-roll regions for the corresponding potential. The classification of different behaviors of  $\bar{\epsilon}$  and  $\bar{\eta}$  will be represented below.

To determine the behavior of slow-roll parameters  $\bar{\epsilon}$  and  $\bar{\eta}$ , we compute their partial derivatives with respect to  $y$ ,

$$\frac{\partial \bar{\epsilon}}{\partial y} = \frac{y^2 v'}{v^3} f(y, \beta), \quad \frac{\partial \bar{\eta}}{\partial y} = \frac{2y}{v^2} g(y, \beta), \quad (17)$$

where

$$\begin{aligned} v' &:= 2y - 3y^2 + 4\beta y^3, \\ f(y, \beta) &:= -2 + 4y - (3 + 2\beta)y^2 + 6\beta y^3 - 4\beta^2 y^4, \\ g(y, \beta) &:= -2 + 6y - (6 + 4\beta)y^2 + 15\beta y^3 - 12\beta^2 y^4. \end{aligned} \quad (18)$$

For  $\beta > 9/32$  we have  $v > 0$  and  $v' > 0$ , so the signature of  $\frac{\partial \bar{\epsilon}}{\partial y}$  or  $\frac{\partial \bar{\eta}}{\partial y}$  depends on the signature of  $f(y, \beta)$  or  $g(y, \beta)$ . In order to determine the signature of  $f$  and  $g$ , we differentiate them with respect to  $y$ ,

$$\begin{aligned} \frac{\partial f}{\partial y} &= 4 - 2(3 + 2\beta)y + 18\beta y^2 - 16\beta^2 y^3, \\ \frac{\partial^2 f}{\partial y^2} &= -48(\beta y - 3/8)^2 - (4\beta - 3/4) < 0, \\ \frac{\partial g}{\partial y} &= 6 - 2(6 + 4\beta)y + 45\beta y^2 - 48\beta^2 y^3, \\ \frac{\partial^2 g}{\partial y^2} &= -144(\beta y - 5/6)^2 - (8\beta - 33/16) < 0. \end{aligned} \quad (19)$$

Since  $\frac{\partial^2 f}{\partial y^2} < 0$  and  $\frac{\partial^2 g}{\partial y^2} < 0$ ,  $\frac{\partial f}{\partial y}$  and  $\frac{\partial g}{\partial y}$  are monotonically decreasing functions of  $y$ . In addition,  $\frac{\partial f}{\partial y}(y = 0) > 0$  and  $\frac{\partial f}{\partial y}(y = \infty) < 0$ , so  $\frac{\partial f}{\partial y}$  has one root in  $(0, \infty)$ . By the same token,  $\frac{\partial g}{\partial y}$  also has one root in  $(0, \infty)$ . We illustrate the previous analysis in Figure 1. From Figure 1 we

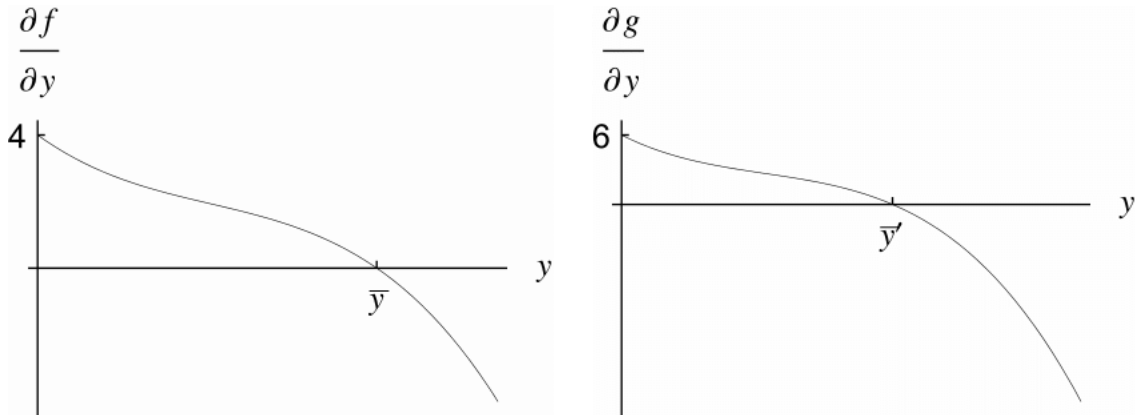


Figure 1: Roots of  $\frac{\partial f}{\partial y}$  and  $\frac{\partial g}{\partial y}$ .

can see that both functions  $f$  and  $g$  have one and only one maximum which is  $\bar{y}$  (respectively  $\bar{y}'$ ) in  $(0, \infty)$ . As  $f(0, \beta) = g(0, \beta) = -2$  and  $f(\infty, \beta)$  or  $g(\infty, \beta) < 0$ , we conclude, (1) if  $f(\bar{y}, \beta) < 0$  (respectively,  $g(\bar{y}', \beta) < 0$ ),  $\bar{\epsilon}$  (respectively,  $\bar{\eta}$ ) is monotonically decreasing in  $(0, \infty)$ ; (2) if  $f(\bar{y}, \beta) > 0$  (respectively,  $g(\bar{y}', \beta) > 0$ ),  $\bar{\epsilon}$  (respectively,  $\bar{\eta}$ ) has one local minimum and one local maximum in  $(0, \infty)$ . Between these two cases, there is an intermediate stage which is  $f(\bar{y}, \beta) = 0$  or  $g(\bar{y}', \beta) = 0$ . As a result, we need to solve following two sets of equations,

$$\left\{ \begin{array}{l} f(y, \beta) = 0 \\ \frac{\partial}{\partial y} f(y, \beta) = 0 \end{array} \right. \quad \text{and} \quad \left\{ \begin{array}{l} g(y, \beta) = 0 \\ \frac{\partial}{\partial y} g(y, \beta) = 0 \end{array} \right. . \quad (20)$$

The two sets of equations are reduced, by a Groebner basis elimination, to

$$(784\beta^3 - 846\beta^2 + 270\beta - 27)(4\beta - 1) = 0 \quad (21)$$

and

$$(8192\beta^3 - 10368\beta^2 + 3591\beta - 378)(25\beta - 6) = 0 \quad (22)$$

respectively. Eq. (22) gives  $\beta = 0.778890$ , which supplies the bounds for the interval in Section 3.1.1, and (21) gives  $\beta = 0.602103$ , which then supplies the bounds for the interval in Section 3.1.2.

### 3.1.1 $\beta \geq 0.7789$

For  $\beta \geq 0.7789$ , both  $\bar{\epsilon}$  and  $\bar{\eta}$  are monotonically decreasing for  $y \in (0, \infty)$ , which is shown in Figure 2. From this graph it can be readily seen that given any  $\nu$  there is only one trivial

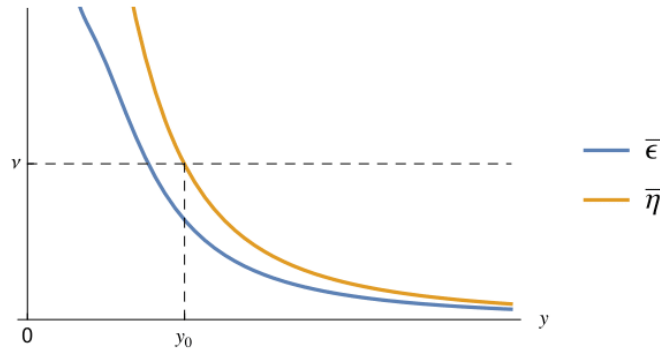


Figure 2: Shapes of  $\bar{\epsilon}$  and  $\bar{\eta}$  for  $\beta \geq 0.7789$ .

slow-roll region for  $y > 0$  which in this graph is  $(y_0, \infty)$ .

### 3.1.2 $0.6021 \leq \beta < 0.7789$

For  $\beta$  in this region,  $\bar{\epsilon}$  is still a monotonically decreasing function for  $y \in (0, \infty)$  while  $\bar{\eta}$  is not any longer. The shape of these two slow-roll parameters are shown in Figure 3. From this graph one

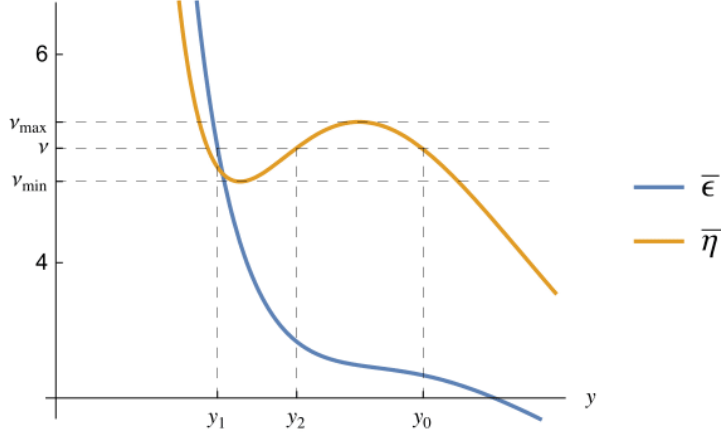


Figure 3: Shapes of  $\bar{\epsilon}$  and  $\bar{\eta}$  for  $0.6021 \leq \beta < 0.7789$ .

can easily read off, given that  $\nu_{\min} < \nu < \nu_{\max}$ , the two slow-roll regions, one of which is  $(y_0, \infty)$  which is trivial, and the other is  $(y_1, y_2)$  which has finite length and is thus the kind of slow-roll region we are searching for. From this graph we can also see that there are an upper bound and a lower bound for  $\nu$  beyond which there is still only one trivial slow-roll region. In fact, this is a common feature, which will be justified in Sections 3.1.3, 3.1.4, and 3.1.5. Therefore, all these bounds of  $\nu$  corresponding to different  $\beta$  render a window opening to non-trivial slow-roll regions, which shall be plotted in Section 3.2.

### 3.1.3 $9/32 \leq \beta < 0.6021$

For  $\beta < 0.6021$ , both  $\bar{\epsilon}$  and  $\bar{\eta}$  are not monotone functions of  $y$  in  $(0, \infty)$ , thus we should expect, on the whole, a wider range of  $\nu$  that opens to non-trivial slow-roll regions. In particular, for  $\beta \in [9/32, 0.6021)$ , the potential  $v$  is still a monotonically increasing function for  $y > 0$ , which means there is no local minimum of  $v$  in  $y \in (0, \infty)$  (the cases that  $v$  has a local minimum in  $y \in (0, \infty)$  shall be dealt with in the following two subsections). The typical shapes of  $\bar{\epsilon}$  and  $\bar{\eta}$  are presented in Figure 4. From this figure, we can see that given  $\nu \in (\nu_{\min}, \nu_{\max})$ , there is a non-trivial slow-roll region,  $(y_1, y_2)$ , apart from the trivial one,  $(y_0, \infty)$ .

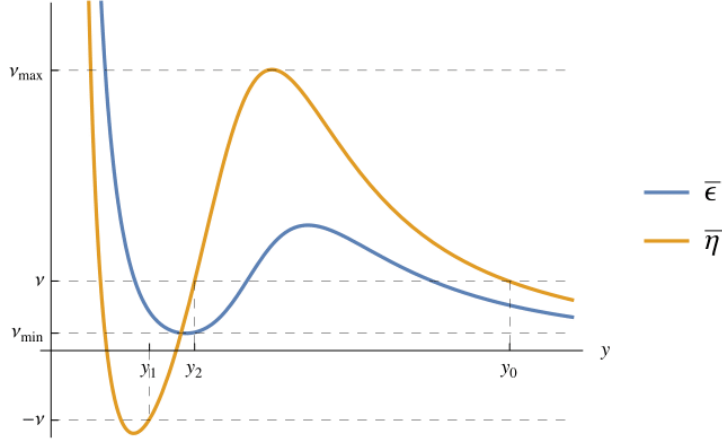


Figure 4: Shapes of  $\bar{\epsilon}$  and  $\bar{\eta}$  for  $9/32 \leq \beta < 0.6021$ .

### 3.1.4 $1/4 < \beta < 9/32$

In this interval,  $v > 0$  still holds, but  $v'$  is not positive definite any longer. So  $\frac{\partial \bar{\epsilon}}{\partial y}$  has two more roots which are the roots of  $v'$ . When  $\beta < 9/32$ , the potential  $v(y)$  has a minimum on the right half  $y - v$  plane. In particular, for  $\beta > 1/4$  this minimum is a local minimum (see the first graph of Figure 5). Physically, we prefer the Universe to not being inflating at the minimum of

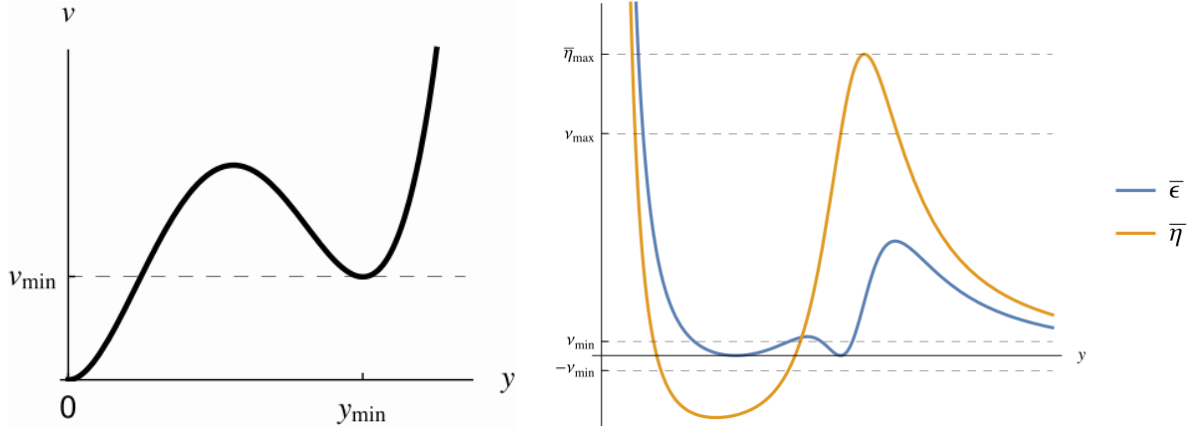


Figure 5: The first graph shows the potential  $v$  has a local minimum at  $y_{\min} > 0$ . The second illustrates typical shapes of  $\bar{\epsilon}$  and  $\bar{\eta}$  for  $1/4 < \beta < 9/32$ .

the potential; the Universe should be reheating and the field should be oscillating. To ensure this, we look for  $|\bar{\eta}(y_{\min})| > \nu$ , where  $y_{\min}$  is the local minimum point of  $v$ . Because of this extra filter, the upper bound of  $\nu$  (viz.,  $\nu_{\max}$ ) is not necessarily equal to the local maximum of  $\bar{\eta}$  (viz.,  $\bar{\eta}_{\max}$ ), which is illustrated in the second graph of Figure 5. In that graph, the lower bound

of  $\nu$ , namely  $\nu_{\min}$ , is also not at the minimum of  $\bar{\epsilon}$  which is 0. This is the consequence of the restriction  $\bar{\eta} > -\nu$ .

### 3.1.5 $0 < \beta \leq 1/4$

Finally, when  $\beta < 1/4$ ,  $v$  in the denominator of (17). This contributes two extra singularities. The potential  $v$  has a true vacuum in the right half  $y - v$  plane, which is shown in the first graph of Figure 6. At this true vacuum, the potential is negative (or zero for  $\beta = 1/4$ ) and thus

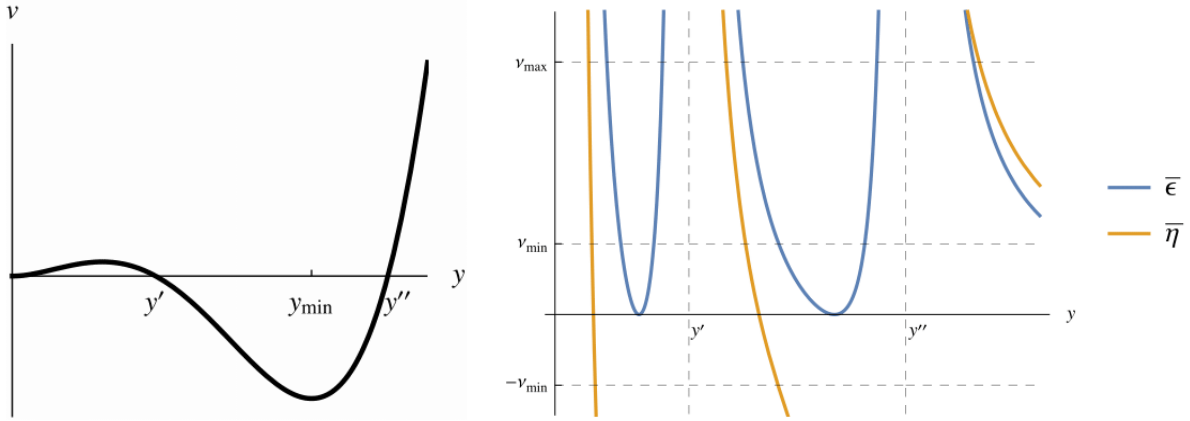


Figure 6: The first graph shows the potential  $v$  has a global minimum at  $y_{\min}$ . The second illustrates typical shapes of  $\bar{\epsilon}$  and  $\bar{\eta}$  for  $0 < \beta < 1/4$ . The  $\beta = 1/4$  case is a special case in which  $y'$  and  $y''$  coincide.

potential  $v(y)$  has two (or one when  $\beta = 1/4$ ) roots, dubbed  $y'$  and  $y''$  respectively.

As a result, the slow-roll parameters  $\bar{\epsilon}$  and  $\bar{\eta}$  are singular at these two roots of  $v$ , which can be seen from the second graph of Figure 6. The bounds of  $\nu$ , namely  $\nu_{\min}$  and  $\nu_{\max}$  are also denoted in that graph.

## 3.2 The window

Now that we have worked out all possible combinations of  $\beta$  and  $\nu$  that opens a window to non-trivial slow-roll potentials whose procedure can be algorithmized by computer programs, we plot the numerical results in Figure 7. There are two salient features in this figure. First, at  $\beta = 1/4$ , the upper bound of  $\nu$  blows up, which means for any large enough  $\nu$  the potential always has a non-trivial slow-roll region. Second, at  $\beta = 9/32$ , there is a discontinuity (jump) in the upper bound of  $\nu$ . This is because, from  $\beta > 9/32$  to  $\beta < 9/32$ , a local minimum

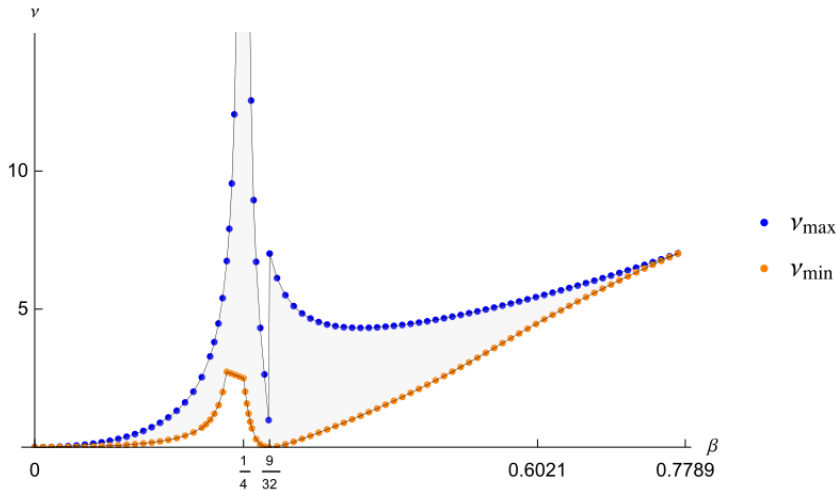


Figure 7: The window that opens to non-trivial slow-roll potentials.

$y_{\min}$  appears suddenly in the potential and the subsequent introduction of the extra constraint  $|\bar{\eta}(y_{\min})| > \nu$  makes the bound of  $\nu$  discontinuous.

## 4 Multi-field models

In this section, we investigate which potentials accommodate the slow-roll conditions for inflation with two fields. The form of the potentials we have is

$$\begin{aligned}
 V(\tilde{\varphi}, \tilde{\chi}) = & \frac{\mu^2}{2} M^2 \tilde{\varphi}^2 + \frac{\rho^2}{2} M^2 \tilde{\chi}^2 + a_1 M \tilde{\varphi}^3 + a_2 M \tilde{\varphi}^2 \tilde{\chi} + a_3 M \tilde{\varphi} \tilde{\chi}^2 + a_4 M \tilde{\chi}^3 \\
 & + b_1 \tilde{\varphi}^4 + b_2 \tilde{\varphi}^2 \tilde{\chi}^2 + b_3 \tilde{\chi}^4,
 \end{aligned} \tag{23}$$

where the masses  $\mu M$  and  $\rho M$  for the fields  $\tilde{\varphi}$  and  $\tilde{\chi}$  are defined in terms of  $M$ , the GUT mass, the  $a_i M$  are cubic couplings, and the  $b_i$  are quartic couplings. We will assume that the masses are around the GUT scale ( $\sim 10^{16}$  GeV). We motivate the quartic potential from a Wilsonian perspective wherein higher order terms are suppressed by the energy scale at which new physics enters. We assume this is the string scale or Planck scale ( $\sim 10^{19}$  GeV). Terms higher than quartic order, as they are suppressed by this higher energy scale, are neglected in the analysis. The coefficients  $a_i$  and  $b_i$  are order one numbers. The terms that appear in (23) are dictated by the fact that we demand all slow-roll potentials to be bounded from below. With this in mind, the  $a_i$  can be positive or negative and the  $b_i$  are positive. When both fields tend to  $-\infty$ , the quartic terms should have no odd powers in any of the two variables. We can rescale (23)

similarly to what we did in the single field case. With  $\tilde{\varphi} = M\varphi$  and  $\tilde{\chi} = M\chi$ , we have

$$v(\varphi, \chi) = \frac{\mu^2}{2}\varphi^2 + \frac{\rho^2}{2}\chi^2 + a_1\varphi^3 + a_2\varphi^2\chi + a_3\varphi\chi^2 + a_4\chi^3 + b_1\varphi^4 + b_2\varphi^2\chi^2 + b_3\chi^4. \quad (24)$$

Now all parameters and variables in potential  $v$  are dimensionless and it is sensible to talk about the magnitude of parameters. Note that  $V = M^4v$ . These methods can readily be generalized to having more scalar fields. We simply require that the superpotential is renormalizable and bounded from below. As adding more scalars and studying the potentials explicitly in the finite field case is computationally more intensive, we do not extend the analysis beyond the two field level in this work. When searching for minima in the potential one will encounter both false and true vacua. We allow for slow-roll regions around false vacua (local minima) and not only the true vacua (global minima). Adding a zeroth order term to the potential will shift the energy of the relative minimum. Though the potential appears in the denominator of the slow-roll conditions, we assume constant terms in the potential do not greatly affect flatness and therefore neglect these terms in writing (24).

#### 4.1 Slow-roll conditions for multi-field inflation

It is important to discuss the slow-roll conditions for multi-field inflation models as they are fundamentally different from those of single field case. The conditions are discussed in detail in [61]. We shall demand the following:

$$\begin{aligned} \epsilon &\equiv -\frac{\dot{H}}{H^2} = 3 \left( \frac{\dot{\phi}_i^2}{V} \right) = \frac{M_{\text{Pl}}^2 (\partial_i V)^2}{2V^2} \ll 1, \\ \xi &\equiv \sqrt{\hat{V}_1 \cdot \overleftrightarrow{\hat{V}}_2 \cdot \overleftrightarrow{\hat{V}}_2 \cdot \hat{V}_1} \ll 1, \end{aligned} \quad (25)$$

with

$$\hat{V}_1 \equiv \frac{\partial_i V}{|\partial_i V|}, \quad \overleftrightarrow{\hat{V}}_2 \equiv \frac{M_{\text{Pl}}^2 (\partial_i \partial_j V)}{V}, \quad (26)$$

for fields  $\phi = (\varphi, \chi)$ . Here the conditions are derived from the approximation  $3H\dot{\phi}_i \approx -\partial_i V$ , which is essentially the consistent second slow-roll condition. This comes down to neglecting  $\ddot{\phi}_i$  compared to  $\partial_i V$ . But when comparing two vectors, it is sensible only to compare their norms. Therefore we have the *strong second slow-roll condition*  $|\ddot{\phi}_i| \ll |\partial_i V|$ . The reason it is called the strong second slow-roll condition is because its smallness implies

$$\eta \equiv \hat{V}_1 \cdot \overleftrightarrow{\hat{V}}_2 \cdot \hat{V}_1 \ll 1, \quad (27)$$



where  $\eta$  is defined to be

$$\frac{1}{\epsilon H} \frac{d\epsilon}{dt} = 4\epsilon - 2\hat{V}_1 \cdot \overleftrightarrow{V}_2 \cdot \hat{V}_1 = 4\epsilon - 2\eta \ll 1. \quad (28)$$

Therefore the slow gradient flow by the fields defined in (25) is not the only way to get a slowly-varying quasi-de Sitter expanding phase.

## 4.2 Numerical tests

In this section, we numerically determine whether a potential of the form (26) satisfies the slow gradient flow condition in (25). Because we now have the free parameters  $\vec{a}$  and  $\vec{b}$ , we will adopt the Monte Carlo paradigm to characterize the shapes of potentials and quantify the rate of success.

### 4.2.1 Setup for numerics

The experiment is set up as follows.

1. The coefficients  $\vec{a}$  and  $\vec{b}$  in cubic and quartic terms in (24) are first sampled from a uniform distribution within range  $[-3, 3]$  and  $[0, 5]$  respectively. In addition, we also sampled the  $\vec{a}$  coefficients from a Gaussian distribution with mean 0 and variance 1, and  $\vec{b}$  coefficients from an exponential distribution with  $\lambda = 1$ .

Let us briefly justify these choices of parameters. The experiments with the uniform distribution are performed in the spirit of Monte Carlo simulations, where parameters are chosen essentially at random. The choice of the uniform distribution is further justified by the fact that we do not know the region where slow-roll solutions reside in the seven dimensional parameter space of the potential coefficients. On the other hand, the choice of normal distribution with particular mean and variance will center our data around that mean and therefore may miss possible slow-roll regions. The choice of uniform distribution reflects the fact that we have no knowledge on the region of slow-roll samples within the parameter space *a priori*. In addition, the parameters are chosen to be of  $O(1)$  with respect to GUT scale. This comes from the fact that the higher order terms of the potential do not get corrections from quantum gravity effects, thereby, the potential is written in this particular quartic form. Note that this polynomial potential allows vertices that mix the two inflatons. This rules out the models such as assisted inflation where potential takes steep exponential [62] due to the fact that our potentials are polynomials.

In the second set of experiments, the Gaussian distribution for  $\vec{a}$  is motivated by the Central Limit Theorem. If we suppose our coefficients can be observed, the averages of  $n$  measurements of each coefficient then approach Gaussian distribution when  $n \rightarrow \infty$ . Meanwhile, the mean and variance are chosen on the grounds of naturalness. *A priori*, the coefficients should be order one numbers at the scale determined by the masses of the inflatons, which we set to GUT scale. Therefore, our choice of Gaussian distribution for  $\vec{a}$  can be seen from previous arguments. On the other hand, we have  $\vec{b}$  follow a Gamma distribution. We demand each of the elements of  $\vec{b}$  to be positive in order to ensure that the potential is bounded from below. Just as the Gaussian distribution is a maximum entropy probability distribution for positive and negative real numbers, the Gamma distribution is the maximum entropy probability distribution for positive real numbers. The Gamma distribution therefore becomes the natural candidate for selecting coefficients. In particular, we use an exponential distribution with  $\lambda = 1$ , which is a Gamma distribution with shape parameter  $k = 1$  and scale parameter  $\theta = \lambda$ . Again, the choice of 1 is motivated on the grounds of naturalness. The Central Limit Theorem requires large  $n$ . It is not clear that this applies when only a small number of scalar fields participate in inflation, so the comparison between the two possibilities is useful.

2. For each set of random coefficients  $\vec{a}$  and  $\vec{b}$ , we search for a point that satisfies conditions (25) within a particular range for fields  $\phi_i$  by using the MATHEMATICA [63] function<sup>2</sup>

$$\mathbf{FindInstance}[\langle \text{slow-roll conditions} \rangle, \{\varphi, \chi\}]. \quad (29)$$

The search region within field space is rectangular with origin in the middle. The size of both sides of this region is twice the maximum of distances between origin and any stationary points of the potential. This is justified because we want a slow-roll region that is near a stationary point and the potential becomes steep far out from the origin in our potentials that are bounded from below. We do not want to falsely classify solutions as slow-roll simply by virtue of the fact the denominator, which is determined by the value of the potential, is large near infinity in field space.

3. For particular conditions in (25), we have observational constraints of

$$\epsilon < 0.01 \quad \text{and} \quad \xi < 0.01 \quad (30)$$

---

<sup>2</sup>Of course, we wrote more code than just this one line function.

from measurements of scalar spectral index  $n_s$  that directly restricts slow-roll parameters. We also note that since the  $\xi$  condition implies  $\eta$ , the results from imposing  $\xi$  should be smaller than those from  $\eta$ .

4. The inflaton mass parameters are defined as  $\mu = m_\varphi/M_{\text{GUT}}$  and  $\rho = m_\psi/M_{\text{GUT}}$ , where  $m_\varphi$  and  $m_\psi$  are the inflaton masses. Here, we set them both to be of GUT scale, so  $\mu$  and  $\rho$  are of order  $O(1)$ . With the mass parameters fixed, we take  $N = 216000$  uniformly distributed random coefficient samples,  $(\vec{a}_1, \vec{b}_1), \dots, (\vec{a}_N, \vec{b}_N)$ . To be precise, we first of all generate 108000 samples using the MATHEMATICA function **RandomReal**[{-3, 3}, 4] for  $\vec{a}$  and **RandomReal**[{0, 5}, 3] for  $\vec{b}$ . Then we apply the slow-roll conditions in (25) to these coefficients using the approach and constraint described in (29) and (30) to obtain instances<sup>3</sup> of relative minima that satisfy the necessary conditions. By noticing that the potential (24) is symmetric under the following transformation for  $\mu = \rho$ ,

$$\varphi \leftrightarrow \chi, \quad a_1 \leftrightarrow a_4, \quad a_2 \leftrightarrow a_3, \quad b_1 \leftrightarrow b_3, \quad (31)$$

we apply this symmetry to the slow-roll coefficients found previously in the 108000 samples. That is equivalently getting all slow-roll coefficients in 216,000 random samples. In addition, this is also done for 50,000, or equivalently, 100,000 samples drawn from Gaussian/Gamma distributions with means and shape parameters chosen as unity.

#### 4.2.2 Numerical results

The statistics of slow-roll potentials we found in potentials from the uniform and Gaussian/Gamma distribution are listed in Table 1. From this table, we can see that in all randomly generated coefficients, around 0.05% of them correspond to slow-roll potentials and 0.1% for Gaussian/Gamma distribution. This supplies a *lower bound* for the percentage of relative minima that accommodate the slow-roll conditions for inflation with two scalar fields.

We also draw distributions of values of coefficients  $(\vec{a}, \vec{b})$  that correspond to slow-roll potentials in Figure 8. These figures show that in spite of the uniform distribution that we presume as priors for  $a_i$  and  $b_i$ , the slow-roll conditions pick the coefficients according to the mass distributions in these histograms. The distributions of all components of  $\vec{a}$  and  $\vec{b}$  deviate noticeably

---

<sup>3</sup>The **FindInstance** function in MATHEMATICA is not capable of finding all desired slow-roll instances due to the mathematical complications of the slow-roll conditions and the internal algorithms designed for this task in MATHEMATICA. Our experimental comparison of **FindInstance** with the more comprehensive but slower **NSolve** function indicate that results from using the two options are similar.

Distribution	Range of $\mathbf{a}$	Range of $\mathbf{b}$	Samples	Slow-Roll	Percentage
Uniform	$[-3, 3]$	$[0, 5]$	108,000	54	0.05%
Gaussian Gamma	$[-\infty, \infty]$	$[0, \infty]$	50,000	50	0.1%

Table 1: Slow-roll potentials found in random sample potentials of chosen distributions

from the uniform distribution. This indicates that the slow-roll conditions set some constraints on the values of coefficients in a probabilistic sense.

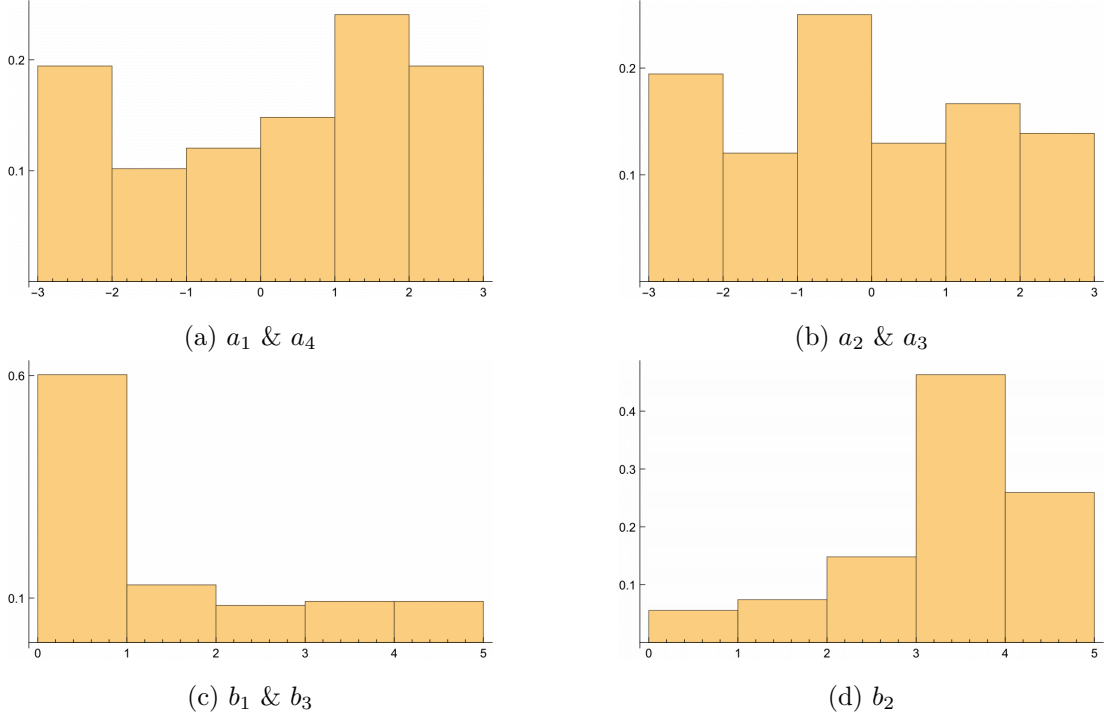
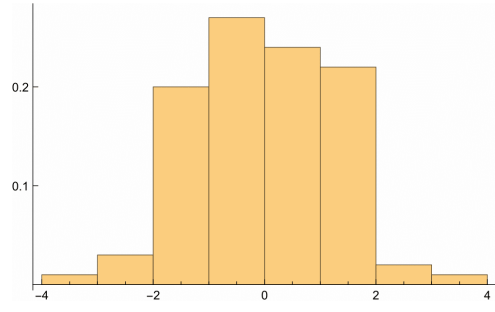


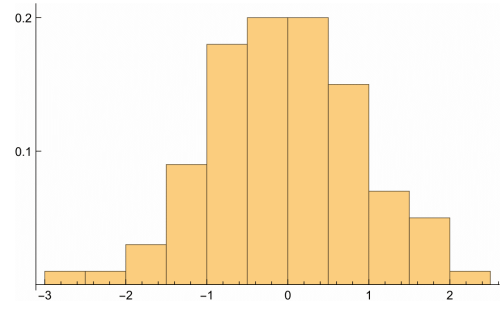
Figure 8: Distribution histogram for  $\vec{a}$  and  $\vec{b}$  coefficients drawn from uniform distribution. The  $x$ -axes are values for  $\vec{a}$  and  $\vec{b}$  and the  $y$ -axes are for probabilities for those values to occur.

In addition to the results from uniform distribution, we also present the histogram plots for coefficients of slow-roll potentials for Gaussian/Gamma distribution in Figure 9. We can see from the plot that the Gaussian nature of the plot still is still present. This shows that the slow-roll conditions we choose respects the Gaussianity of initial samples.

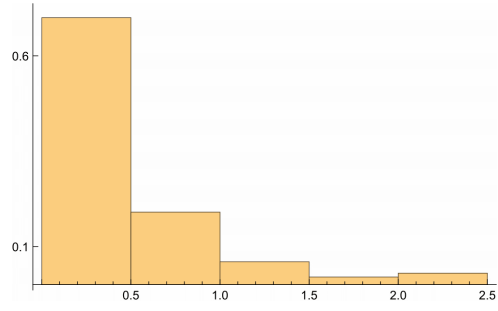
Preliminary experiments with varying the mass parameters for the scalar fields over several orders of magnitude do not significantly change the percentages of slow-roll solutions.



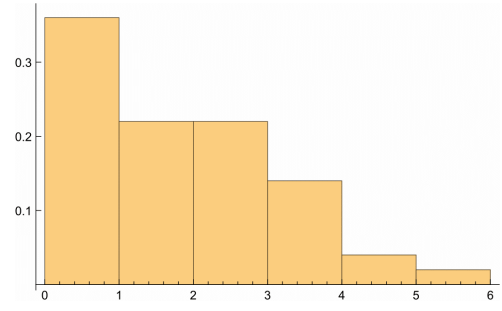
(a)  $a_1$  &  $a_4$



(b)  $a_2$  &  $a_3$



(c)  $b_1$  &  $b_3$



(d)  $b_2$

Figure 9: Distribution histogram for  $\vec{a}$  and  $\vec{b}$  coefficients drawn from Gaussian/Gamma distribution. The  $x$ -axes are values for  $\vec{a}$  and  $\vec{b}$  and the  $y$ -axes are for probabilities for those values to occur.

## 5 Discussion and outlook

With the advent of Big Data in theoretical physics and ever-increasing computational power, we are gaining further glimpses into the various landscapes of theories ranging from string vacua to cosmological scenarios. In this paper, we have been motivated by the question of the probability of having slow-roll inflation within the landscape of effective potentials for inflatons.

We started with the case of a single field with the most generic form of the potential up to degree four, subject to the constraints of slow-roll. Here, there are only two parameters, which we have dubbed  $\beta$  and  $\nu$ , and which can be expressed in terms of the couplings. We can solve the problem numerically to arrive at Figure 7. The figure depicts a non-trivial region of parameter values which satisfy the slow-roll conditions.

With two inflatons, the situation is understandably more intricate. Here, up to degree four, there are seven parameters. The slow-roll conditions then translate to a polynomial system in the fields and in the parameters. This is then a problem in a potential landscape sculpted by these parameters. We find that the slow-roll conditions for multi-field are insensitive to the distribution we used, *i.e.*, we find that they give the same percentage of slow-roll instances.

In the single field case, the condition  $V' V''' \ll V^2 M_{\text{P}}^{-4}$  accounts for constraints on the running of the spectral index. It would be reasonable to develop the equivalent third derivative condition for multi-field case and include this within the framework of random potentials. In addition, in this work we do not explicitly compute the number of  $e$ -foldings for each of the potentials that support slow-roll inflation. While we can exclude certain minima as being unable to support the necessary number of  $e$ -foldings, the suitability of other minima for this purpose depends critically on the choice of initial conditions for the inflaton fields. There is no obvious *a priori* selection criteria for this informed by realistic string constructions of the Standard Model. We defer a systematic analysis on this point for future work.

In general, with an arbitrary number of inflatons and a potential up to a specified degree, the slow-roll constraints will produce a large polynomial system with still larger number of parameters. For example, in the heterotic string Standard Models to which we alluded in the introduction, the contribution to the number of moduli fields come from the geometry — roughly the sum of the Hodge numbers — and from the bundle — roughly the number of endomorphisms [64]. For the  $(3, 3)$  Calabi–Yau threefold studied in [8, 9] the total number of moduli is  $6 + 19 = 25$ .

The usual Groebner basis [65] approach to analyzing such systems will soon become rather

prohibitive and even numerical algebraic geometry [59] will find this challenge daunting. Our approach of randomization over parameters is thus the standard technique, and the statistics over the landscape is an enlightening overview of how special or generic our universe is.

One should mention also that there is a branch of mathematics known as random algebraic geometry where the usual quantities such topological invariants and cohomology, which govern the physics, have their analogues in the stochastic sense. It will certainly be interesting to study polynomial systems arising from the potential landscape under this light.

## Acknowledgements

We thank Cyril Matti for collaboration during an early stage of this work. YHH would like to thank the Science and Technology Facilities Council, UK, for grant ST/J00037X/1, the Chinese Ministry of Education, for a Chang-Jiang Chair Professorship at NanKai University as well as the City of Tian-Jin for a Qian-Ren Scholarship, and Merton College, Oxford, for her enduring support. VJ and LP are supported by the South African Research Chairs Initiative, which is funded by the Department of Science and Technology and the National Research Foundation of South Africa. YX is support by the Doctoral Studentship of City University of London. DZ is supported by the China National Natural Science Foundation under contract No. 11105138 and 11575177. DZ is also indebted to Chinese Scholarship Council (CSC) for support.

## References

- [1] A. A. Starobinsky, Phys. Lett. **91B**, 99 (1980).
- [2] A. H. Guth, Phys. Rev. D **23**, 347 (1981).
- [3] A. D. Linde, Phys. Lett. **108B**, 389 (1982).
- [4] A. Albrecht and P. J. Steinhardt, Phys. Rev. Lett. **48**, 1220 (1982).
- [5] D. H. Lyth and A. Riotto, Phys. Rept. **314**, 1 (1999). [hep-ph/9807278].
- [6] J. Martin, C. Ringeval and V. Vennin, Phys. Dark Univ. **5-6**, 75 (2014). [arXiv:1303.3787 [astro-ph.CO]].
- [7] P. Candelas, G. T. Horowitz, A. Strominger and E. Witten, Nucl. Phys. B **258**, 46 (1985).

- [8] V. Braun, Y. H. He, B. A. Ovrut and T. Pantev, Phys. Lett. B **618**, 252 (2005). [hep-th/0501070].
- [9] V. Braun, Y. H. He, B. A. Ovrut and T. Pantev, JHEP **0605**, 043 (2006). [hep-th/0512177].
- [10] V. Bouchard and R. Donagi, Phys. Lett. B **633**, 783 (2006). [hep-th/0512149].
- [11] L. B. Anderson, J. Gray, A. Lukas and E. Palti, Phys. Rev. D **84**, 106005 (2011). [arXiv:1106.4804 [hep-th]].
- [12] L. B. Anderson, J. Gray, A. Lukas and E. Palti, JHEP **1206**, 113 (2012). [arXiv:1202.1757 [hep-th]].
- [13] M. Kreuzer and H. Skarke, Commun. Math. Phys. **185**, 495 (1997). [hep-th/9512204].
- [14] <http://hep.itp.tuwien.ac.at/~kreuzer/CY/>
- [15] V. V. Batyrev, J. Alg. Geom. **3**, 493 (1994). [alg-geom/9310003].
- [16] V. V. Batyrev and L. A. Borisov, [alg-geom/9412017].
- [17] R. Altman, J. Gray, Y. H. He, V. Jejjala and B. D. Nelson, JHEP **1502**, 158 (2015). [arXiv:1411.1418 [hep-th]].
- [18] <http://www.rossealtman.com/>
- [19] G. 't Hooft, NATO Sci. Ser. B **59**, 135 (1980).
- [20] Y. H. He, V. Jejjala and L. Pontiggia, [arXiv:1512.01579 [hep-th]].
- [21] M. Grana, Phys. Rept. **423**, 91 (2006). [hep-th/0509003].
- [22] M. R. Douglas and S. Kachru, Rev. Mod. Phys. **79**, 733 (2007). [hep-th/0610102].
- [23] I. Bena, M. Graña, S. Kuperstein and S. Massai, JHEP **1502**, 146 (2015). [arXiv:1410.7776 [hep-th]].
- [24] H. Ooguri and C. Vafa, [arXiv:1610.01533 [hep-th]].
- [25] B. Freivogel and M. Kleban, [arXiv:1610.04564 [hep-th]].
- [26] G. Hinshaw *et al.* [WMAP Collaboration], Astrophys. J. Suppl. **208**, 19 (2013). [arXiv:1212.5226 [astro-ph.CO]].



- [27] P. A. R. Ade *et al.* [Planck Collaboration], *Astron. Astrophys.* **594**, A13 (2016).  
[arXiv:1502.01589 [astro-ph.CO]].
- [28] P. A. R. Ade *et al.* [Planck Collaboration], *Astron. Astrophys.* **594**, A20 (2016).  
[arXiv:1502.02114 [astro-ph.CO]].
- [29] A. D. Linde, *Phys. Rev. D* **49**, 748 (1994). [astro-ph/9307002].
- [30] D. Baumann and L. McAllister, [arXiv:1404.2601 [hep-th]].
- [31] M. R. Douglas, *JHEP* **0305**, 046 (2003). [hep-th/0303194].
- [32] F. Denef and M. R. Douglas, *JHEP* **0405**, 072 (2004). [hep-th/0404116].
- [33] M. R. Douglas, *Comptes Rendus Physique* **5**, 965 (2004). [hep-th/0409207].
- [34] F. Denef and M. R. Douglas, *JHEP* **0503**, 061 (2005). [hep-th/0411183].
- [35] A. Aazami and R. Easther, *JCAP* **0603**, 013 (2006). [hep-th/0512050].
- [36] R. Easther and L. McAllister, *JCAP* **0605**, 018 (2006). [hep-th/0512102].
- [37] A. J. Bray and D. S. Dean, *Phys. Rev. Lett.* **98**, 150201 (2007).
- [38] J. Frazer and A. R. Liddle, *JCAP* **1102**, 026 (2011). [arXiv:1101.1619 [astro-ph.CO]].
- [39] D. Marsh, L. McAllister and T. Wrase, *JHEP* **1203**, 102 (2012). [arXiv:1112.3034 [hep-th]].
- [40] D. Battefeld, T. Battefeld and S. Schulz, *JCAP* **1206**, 034 (2012). [arXiv:1203.3941 [hep-th]].
- [41] T. C. Bachlechner, D. Marsh, L. McAllister and T. Wrase, *JHEP* **1301**, 136 (2013).  
[arXiv:1207.2763 [hep-th]].
- [42] I. S. Yang, *Phys. Rev. D* **86**, 103537 (2012). [arXiv:1208.3821 [hep-th]].
- [43] F. G. Pedro and A. Westphal, *Phys. Lett. B* **739**, 439 (2014). [arXiv:1303.3224 [hep-th]].
- [44] M. C. D. Marsh, L. McAllister, E. Pajer and T. Wrase, *JCAP* **1311**, 040 (2013).  
[arXiv:1307.3559 [hep-th]].
- [45] G. Wang and T. Battefeld, *JCAP* **1604**, no. 04, 025 (2016). [arXiv:1512.04224 [hep-th]].

- [46] A. Masoumi and A. Vilenkin, JCAP **1603**, no. 03, 054 (2016). [arXiv:1601.01662 [gr-qc]].
- [47] F. G. Pedro and A. Westphal, [arXiv:1611.07059 [hep-th]].
- [48] R. Easther and L. C. Price, JCAP **1307**, 027 (2013). [arXiv:1304.4244 [astro-ph.CO]].
- [49] J. Frazer and A. R. Liddle, JCAP **1202**, 039 (2012). [arXiv:1111.6646 [astro-ph.CO]].
- [50] J. Frazer, JCAP **1401**, 028 (2014). [arXiv:1303.3611 [astro-ph.CO]].
- [51] R. Easther, J. Frazer, H. V. Peiris and L. C. Price, Phys. Rev. Lett. **112**, 161302 (2014). [arXiv:1312.4035 [astro-ph.CO]].
- [52] B. Greene, D. Kagan, A. Masoumi, D. Mehta, E. J. Weinberg and X. Xiao, Phys. Rev. D **88**, no. 2, 026005 (2013). [arXiv:1303.4428 [hep-th]].
- [53] M. Dine and S. Paban, JHEP **1510**, 088 (2015). [arXiv:1506.06428 [hep-th]].
- [54] M. Dine, [arXiv:1512.08125 [hep-th]].
- [55] A. Masoumi, A. Vilenkin and M. Yamada, [arXiv:1612.03960 [hep-th]].
- [56] R. Easther, A. H. Guth and A. Masoumi, [arXiv:1612.05224 [hep-th]].
- [57] A. Linde, [arXiv:1612.04505 [hep-th]].
- [58] A. Masoumi, A. Vilenkin and M. Yamada, [arXiv:1704.06994 [hep-th]].
- [59] Y. H. He, D. Mehta, M. Niemerg, M. Rummel and A. Voleanu, JHEP **1307**, 050 (2013) doi:10.1007/JHEP07(2013)050 [arXiv:1301.0946 [hep-th]].
- [60] M. Jain and V. Vanchurin, JHEP **1601**, 107 (2016). [arXiv:1506.03840 [hep-th]].
- [61] I. S. Yang, Phys. Rev. D **85**, 123532 (2012). [arXiv:1202.3388 [hep-th]].
- [62] A. R. Liddle, A. Mazumdar and F. E. Schunck, Phys. Rev. D **58**, 061301 (1998). [astro-ph/9804177].
- [63] Wolfram Research, Inc., Mathematica, Version 10.0, Champaign, IL (2014).
- [64] E. I. Buchbinder, R. Donagi and B. A. Ovrut, Nucl. Phys. B **653**, 400 (2003) doi:10.1016/S0550-3213(02)01093-3 [hep-th/0205190].

- [65] J. Gray, Y. H. He, A. Ilderton and A. Lukas, *Comput. Phys. Commun.* **180**, 107 (2009)  
doi:10.1016/j.cpc.2008.08.009 [arXiv:0801.1508 [hep-th]].